In Vitro and In Vivo Detection of Functional Somatostatin Receptors in Canine Insulinomas

Joris H. Robben, Heleen A. Visser-Wisselaar, Gerard R. Rutteman, Peter P. van Rijk, Alice J. van Dongen, George Voorhout, Ted S.G.A.M. van den Ingh, Leo J. Hofland and Steven W.J. Lamberts

Departments of Clinical Sciences of Companion Animals, Radiology and Pathology, Faculty of Veterinary Medicine, Utrecht University, Utrecht; Department of Nuclear Medicine, University Hospital Utrecht, Utrecht; Department of Internal Medicine III, University Hospital Dijkzigt, Rotterdam, The Netherlands

Ten dogs with hypoglycemia due to insulinomas were studied to assess the expression of somatostatin receptors (SSTRs) in canine insulinomas and its potential diagnostic value. **Methods:** The response of circulating glucose and insulin concentrations to the subcutaneous administration of a somatostatin analog, octreotide, was measured. SSTRs were visualized in vitro by autoradiography. [Iodine-125-Tyr^3]-octreotide and [^{125}I-Tyr^{11}]-somatostatin-14 (SRIF-14) were used as radioligands. SPECT was performed 6 hr after the injection of [^{111}In-DTPA-D-Phe^1]-octreotide. **Results:** After subcutaneous injection of 50 μg octreotide, plasma glucose concentration rose from 2.3 ± 0.2 mmol/liter to 3.2 ± 0.3 mmol/liter at 3.5 hr ($p < 0.05$) and plasma insulin concentration decreased from 451 ± 135 pmol/liter to a nadir of 249 ± 115 pmol/liter at 30 min ($p < 0.05$). In vitro autoradiography revealed that all primary insulinomas and their metastases had specific SSTRs for both [^{125}I-Tyr^3]-octreotide and [^{125}I-Tyr^{11}]-SRIF-14. Scatchard analysis of SSTR binding in the tumor tissue of one dog revealed high-affinity binding sites for [^{125}I-Tyr^3]-octreotide (dissociation constant (Kd) 1.7 n*M*, maximum binding capacity (Bmax) 499 fmol/mg membrane protein). The primary tumor and/or metastases in five of six dogs could be visualized and localized by SPECT with [^{111}In-DTPA-D-Phe^1]-octreotide. In the remaining dog, multiple metastases (<3 mm) were found in the liver at necropsy, apparently too small to be visualized by SPECT. **Conclusion:** The in vitro autoradiography and ligand binding studies indicate that canine insulinomas express one type of SSTR. This is in contrast with findings in humans where, on the basis of ligand binding studies, different subtypes of SSTRs have been identified. The uniformity of SSTRs, their high frequency of expression and the high incidence of metastatic disease make canine insulinomas very suitable for investigation of the value of SRIF analogs in the diagnosis and treatment of metastasized endocrine pancreatic tumors.

Key Words: somatostatin; octreotide; dog; insulinomas; receptor imaging

J Nucl Med 1997; 38:1036–1042

The incidence of human insulinoma is four cases per one million person-years (*1*). About 80%–90% of human insulinomas are benign, and surgery is the treatment of choice (*2*). Localization of the primary tumor and clinical staging help the clinician plan treatment and predict the prognosis (*1*). Preoperative noninvasive imaging techniques such as ultrasonography, CT and MRI have been disappointing in visualizing and staging insulinomas (*2,3*). During the last decade in vitro and in vivo imaging of somatostatin receptors (SSTRs) has added a new dimension to the diagnostic procedures.

Various neuroendocrine tumors express receptors that bind somatostatin (SRIF) or its analog octreotide with high affinity, as was demonstrated by classical biochemical ligand binding techniques and in vitro autoradiography (*4–7*). The intravenous administration of [^{123}I-Tyr^3]-octreotide or [^{111}In-DTPA-d-Phe^1]-octreotide facilitates the in vivo visualization of SSTR-positive tumors (*8–11*). Most primary endocrine pancreatic tumors and their metastases can be visualized in this way (*12,13*).

SRIF analogs also can be used therapeutically if the primary tumor cannot be identified, if surgical resection is unsuccessful or if there is metastatic disease. The SRIF analog may reduce hormone secretion, relieve signs and symptoms, and inhibit tumor growth. However, most studies on inhibition of tumor growth have dealt with in vitro cell lines or transplanted tumors (*14–16*). Furthermore, radiotherapy with an α- or β-emitting isotope-coupled SRIF analog has been suggested as a therapeutic option (*7,17*).

Canine insulinomas comprise a valuable in vivo model to study the effectiveness of SRIF or its analogs in the diagnosis and treatment of malignant endocrine pancreatic tumors. Insulinoma is the most common tumor of the endocrine pancreas in dogs. As in man, its incidence is low, but the occurrence of visible metastases is as high as 45% at the time of diagnosis (*18,19*). Hence, this animal model is especially suitable for study of the therapeutic effectiveness of SRIF analogs in metastatic disease.

This study was designed to investigate the expression of SSTRs in canine insulinomas and to assess its diagnostic application. The response of circulating glucose and insulin concentrations to the subcutaneous administration of a single dose of octreotide was measured in dogs with insulinomas. The presence of SSTRs in tumor tissue was studied both in vitro and in vivo. For the in vivo detection of SSTRs in tumors, scintigraphy was performed after the injection of [^{111}In-DTPA-d-Phe^1]-octreotide. The results were compared with findings at surgery and/or autopsy.

MATERIALS AND METHODS

Dogs

We studied 10 dogs with recently observed signs of hypoglycemia (Tables 1 and 2). All were primary cases except Dog 2. This dog was presented with signs of hypoglycemia 1.5 yr after surgery for insulinoma and subsequent treatment with alloxan. Treatment of the alloxan-induced diabetes mellitus with insulin had been discontinued shortly before the second referral. The principal signs of hypoglycemia were seizures, episodic weakness and ataxia. Other signs (Table 2) were less frequent and usually accompanied these signs. In all dogs the results of routine laboratory examinations were within reference ranges except for plasma glucose levels, which were below the reference range of 3.9–5.0 mmol/liter. The diagnosis of insulin-secreting β-cell tumor was based on the combination of a low-plasma glucose level and a relatively high-plasma insulin level (*20,21*).

Received Mar. 12, 1996; revision accepted Sep. 19, 1996.

For correspondence or reprints contact: Joris H. Robben, Department of Clinical Sciences of Companion Animals, Faculty of Veterinary Medicine, Utrecht University, P.O. Box 80.154, 3508 TD, Utrecht, The Netherlands.

TABLE 1
Signalments and Sites of Primary Tumors and Their Metastases in 10 Dogs with Insulinomas

Dog no.	Breed	Age (yr)	Sex	Diagnosis	Pancreatic site	Regional lymph nodes	Liver	Others
1	Mixed breed	10	FS	A	?	+	–	+*
2	Boxer	12	FS	S	–	–	+	+†
3	Scottish sheepdog	10	M	A	L	+	+	–
4	Mixed breed	11	M	S	L	–	–	–
5	German pointer	8	M	S	R	–	–	–
6	Mechelen shepherd	10	M	S/A	L	–	–	–
7	Mixed breed	5	FS	S/A	L	+	+	–
8	Labrador retriever	7	M	S	L	+	–	–
9	Golden retriever	15	M	A	?	–	+	–
10	Golden retriever	11	FS	A	C	+	+	–

*Metastasis in the heart.
†Regional metastasis with concomitant old hemorrhage and necrosis.
FS = spayed female; M = male; A = diagnosis confirmed by necropsy; S = diagnosis confirmed by surgery; + = tumour tissue found; – = no tumor tissue found; ? = site unknown; L = left pancreatic lobe; R = right pancreatic lobe; C = pancreatic corpus.

Blood samples were collected by jugular venipuncture in oxalate-fluoride-coated tubes for measurement of plasma glucose concentration and in precooled EDTA-coated tubes for measurement of plasma insulin concentration. The latter samples were centrifuged at 4°C and plasma was stored at −20°C until used for assay. The glucose concentration in plasma was measured with a modified Trinder method on a Wako 20R discrete analyzer (Wako Chemicals, Neuss, Germany) (*22*). Plasma insulin concentration was determined by a double-antibody RIA (MedGenix Diagnostics, Brussels, Belgium) with an intra-assay variation of 5.3% and an interassay variation of 6.0%. Serial dilutions of a canine plasma were parallel to the standard curve of human insulin. A reference range for basal plasma insulin was determined in eight clinically normal dogs which were withheld food for 3 hr before sampling, as were the dogs with insulinomas.

Ultrasonographic examination of the abdomen was performed in all dogs by use of a real-time mechanical sector scanner (ATL Mark 300; Advanced Technology Laboratories, Woerden, The Netherlands) with a 5.0-MHz transducer. All ultrasonographic examinations were performed by one of the authors who has extensive experience in veterinary ultrasonography.

Tissue specimens were collected by surgical resection and/or at necropsy immediately after euthanasia. Specimens of 5–15 mm in diameter were obtained from the primary tumor, apparent metastases and macroscopically unaffected pancreas. They were frozen in liquid nitrogen and stored at −70°C. Specimens for histological examination were collected immediately adjacent to the specimens that were frozen.

TABLE 2
Presenting Signs in 10 Dogs with Insulinomas

Clinical signs	Number of dogs
Seizures	7
Ataxia	7
Weakness	6
Increased drinking and urinating	5
Increased weight	4
Polyphagia	3
Nervousness	3
Muscle fasciculations	2
Exercise intolerance	2
Collapse	1
Posterior paresis	1
Panting	1

Octreotide Test

The octreotide test was performed in eight dogs. Food was withheld for 3 hr before the test and during the test period of 4 hr. Blood was collected for measurement of plasma glucose concentration immediately before and at 30, 60, 120, 150, 180, 210 and 240 min after the subcutaneous administration of 50 μg octreotide (SMS 201–995; Sandostatin, Sandoz Pharmaceutical, Basel, Switzerland). Plasma insulin concentration was measured in samples collected at 0, 15, 30, 60, 120 and 240 min.

In Vitro Visualization of Somatostatin Receptors

SSTRs were visualized by autoradiography in frozen sections of tissue, as described previously (*5*). [Iodine-125-Tyr^3]-octreotide and [^{125}I-Tyr^{11}]-somatostatin-14 (SRIF-14) (Amersham, Little Chalfont, England) were used as radioligands.

For autoradiography 10-μm sections were cut on a cryostat (Jung CM3000, Leica, Germany), mounted on precleaned gelatin-coated microscope slides and stored at −80°C. To wash out endogenous somatostatin, the sections were preincubated for 10 min at room temperature in 170 m*M* Tris-HCl, pH 7.4. They were then incubated for 1 hr ([^{125}I-Tyr^3]-octreotide) or 30 min ([^{125}I-Tyr^{11}]-SRIF-14) at 20°C in 170 m*M* Tris-HCl buffer, pH 7.4, containing 1% BSA, bacitracin (40 μg/ml), and $MgCl_2$ (5 m*M*) to inhibit endogenous proteases in the presence of iodinated ligand (0.16×10^6 dpm/ml or about 80–160 p*M*). Nonspecific binding was determined in duplicate sections by adding unlabeled [Tyr^3]-octreotide or [Tyr^{11}]-SRIF-14 in a concentration of 1 μM. After incubation, the sections were washed twice for 5 min in cold 170 m*M* Tris-HCl buffer, pH 7.4, containing 0.25% BSA, and once in 170 m*M* Tris-HCl, pH 7.4. The sections were washed in distilled water to remove salt, dried quickly and exposed to Hyperfilm^{TM}-^{3}H (Amersham) for four days in radiograph cassettes without intensifying screens at −80°C. For histological examination, sequential cryosections were stained with hematoxylin and azophloxine.

Somatostatin Receptor Binding Studies

The method of membrane isolation and the reaction conditions were the same as those described by Reubi (*23*). The radioligand used in the binding studies was the ^{125}I-labeled SRIF analog [Tyr^3]-octreotide. Briefly, membrane preparations (corresponding to 30–50 μg protein) were incubated in a total volume of 100 μl at

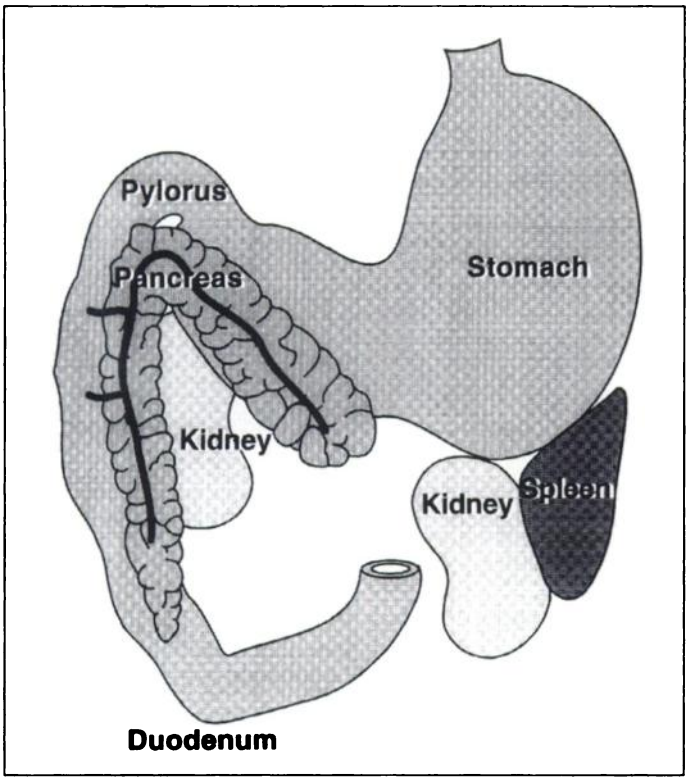

FIGURE 1. Schematic drawing of the canine abdomen, ventral view. The pancreas has two lobes that are united at the body. The body is located near the gastric pylorus, adjacent to the right abdominal wall in the ninth intercostal space. The left lobe passes caudosinistrally to the level of the cranial pole of the left kidney. The right lobe lies along the descending duodenum, extending as far as the caudal pole of the left kidney (*26*).

room temperature for 60 min with 40,000 cpm (approximately 0.15 n*M*) radioligand and increasing concentrations of unlabeled [Tyr^3]-octreotide in HEPES buffer (10 m*M* HEPES, 5 m*M* $MgCl_2$, and bacitracin (0.02 g/L, pH 7.6) containing 0.2% BSA (Boehringer Mannheim B.V., Mannheim, Germany). After the incubation, 1 ml ice-cold HEPES buffer (pH 7.6) was added to the reaction mixture and membrane-bound and unbound radioactivity were separated by centrifugation for 2 min at 14,000 rpm in an Eppendorf microcentrifuge (*24*). The pellet was washed twice with ice-cold HEPES buffer, and radioactivity in the final pellet was measured in a gamma counter. SSTR binding data were analyzed by the method of Scatchard (*25*).

In Vivo Somatostatin Receptor Imaging

For scintigraphy, the dogs were anesthetized by intravenous injection of medetomidine (Domitor; Orion Corporation Farmos, Turku, Finland) and propofol (Diprivan; Zeneca B.V., Ridderkerk, The Netherlands).

Six dogs received 80 MBq [^{111}In-DTPA-d-Phe^1]-octreotide (Mallinckrodt Medical, Petten, The Netherlands) intravenously, 6 hr before scintigraphy. Synthesis, radiolabeling and in vitro and in vivo validation of the product have been described (*9,10*). SPECT images were obtained during a period of 35 min (20 steps at 6° angulation with 80-sec acquisition per step in a 64 × 64 matrix) with a three-head gamma camera (Picker Prism 3000, Cleveland, Ohio) equipped with medium-energy, parallel-hole collimators. The resolution of the camera was 10 mm FWHM. The photopeak windows used were 171 keV at 15% and 243 keV at 25%. Reconstruction was performed without scatter correction. Projections were prefiltered with a Wiener filter, cutoff 0.2, and transverse reconstruction of single-pixel slices was performed with a Ramp filter. Attenuation correction was performed assuming uniform attenuation with an ellipse drawn around the body.

The field of view covered the abdomen from the diaphragm to the cranial pole of the left kidney (Fig. 1). Therefore, in most dogs the caudal pole of the right pancreatic lobe was outside the field of view. Primary concern for localizing hepatic metastases and the limited field of view determined the window used.

Statistical Analysis

The results of the octreotide test are presented as mean ± s.e.m. The hypothesis of no time effect for plasma glucose and insulin levels was tested by univariate analysis of variance for repeated measures. Planned contrasts between the first and after time points were tested by the F-statistic. To control for Type I errors due to unequal variances for each test occasion or variable correlations for different pairs of test occasions, degrees of freedom were adjusted from $F^{(k-1)}_{(R1)(n-1)}$ to $F^{1}_{(n-1)}$ (k=number of time points, n = number of dogs). A probability of < 0.05 was considered significant.

RESULTS

Dogs

In all dogs basal plasma glucose concentration (2.3 ± 0.2 mmol/liter) was below the reference range (3.9–5.0 mmol/liter). Basal plasma insulin concentration (538 ± 122 pmol/liter) varied from 108-1278 pmol/liter (Table 3). Dogs 3–5 and 9 (Table 3) had basal insulin concentrations within the reference range of 43–345 pmol/liter (mean 170 ± 37 pmol/liter), despite glucose levels below the reference range.

Ultrasonography was unsuccessful in imaging the pancreatic region and the liver in Dog 1 and the pancreatic region in Dogs 5, 7 and 8, due to gas in the gastrointestinal tract and/or an abundance of intra-abdominal fat. No abnormalities were found in the livers of Dogs 5, 7 and 8. In Dogs 4, 9 and 10, no abnormalities were found in the pancreatic region, but hypoechoic (Dogs 4 and 9) or hyperechoic (Dog 10) lesions were found in the liver. In Dogs 2, 3 and 6, space-occupying lesions were found in the pancreatic region, isoechoic or hypoechoic to liver, with diameters of 3.0, 2.5 and 1.5 cm, respectively. Examination of the livers revealed multiple ill-defined hyperechoic and well-defined hypoechoic areas in Dog 2, a slightly hyperechoic lesion with a diameter of 4 cm in Dog 3 and no abnormalities in Dog 6.

Results of histological examination of tissue specimens confirmed the presence of endocrine pancreatic tumor in all dogs (Table 1). When these results were compared with those of ultrasonography, it was apparent that the primary tumors in Dogs 1, 4, 5 and 7–10 were not visualized with this technique. The nodule in the pancreatic region of Dog 2 proved to be a metastatic tumor with an organized hematoma. Metastases in regional lymph nodes (2–4 cm in diameter) were not visualized in Dogs 1, 3, 7, 8 and 10. The hypoechoic lesions in the liver of Dog 4 were not caused by tumor tissue, the liver metastases (<3 mm) in Dog 7 had not been visualized and the extent of the liver metastases in Dogs 3 and 9 had been underestimated.

Octreotide Test

None of the dogs had clinical signs of hypoglycemia during or after the test. Mean plasma glucose levels increased from 2.3 ± 0.3 mmol/liter to 3.2 ± 0.3 mmol/liter at 210 min ($p < 0.05$) and to 2.9 ± 0.3 mmol/liter at 240 min ($p < 0.05$) after administration of the octreotide (Fig. 2), although normal or elevated glucose levels were achieved in only two dogs during the test. Plasma insulin levels decreased from 451 ± 135 pmol/liter to a nadir at 15 and 30 min (249 ± 122 and 249 ± 115 pmol/liter, respectively), representing a decrease of 44% ± 7% below the basal levels (Table 3). This significant decrease ($p < 0.05$) was followed by a gradual rise in plasma insulin levels (Fig. 2).

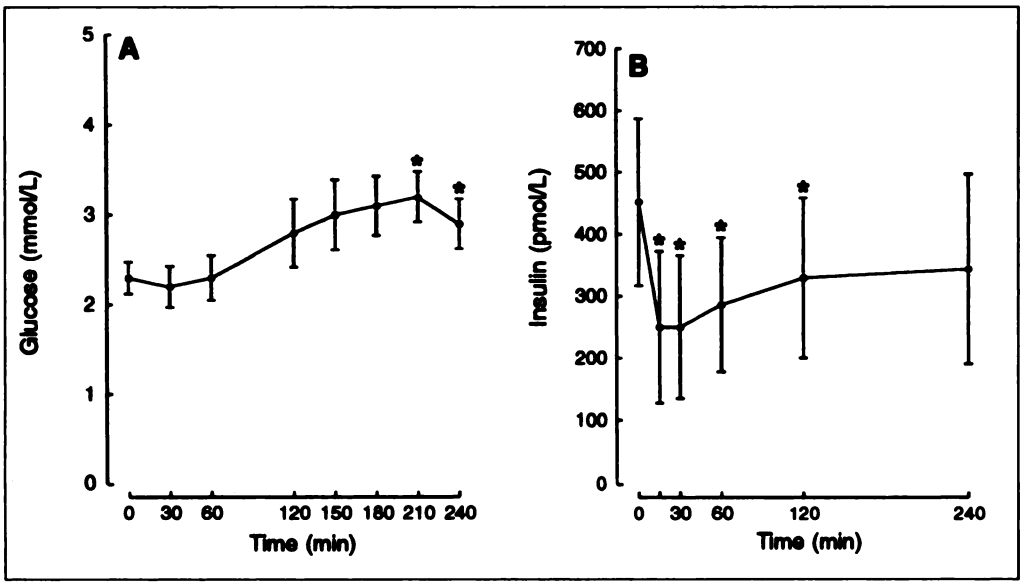

FIGURE 2. (A) Plasma glucose and (B) plasma insulin responses to subcutaneous administration of 50 μg octreotide in eight dogs with insulinomas. Results are expressed as mean ± s.e.m. * Significantly different from levels at 0 min.

In Vitro Visualization of Somatostatin Receptors

Autoradiography revealed that all tumor tissues from the 10 dogs had binding sites for both [^{125}I-Tyr^{11}]-SRIF-14 and [^{125}I-Tyr^{3}]-octreotide (Table 3). The [Tyr^{3}]-octreotide and [Tyr^{11}]-SRIF-14 binding sites were distributed uniformly throughout the tumor tissues. Histological examination of cryostat sections adjacent to those used for autoradiography confirmed the presence of epithelial tumor tissue in SSTR-positive areas (Fig. 3A). Areas not containing SSTRs proved to be normal pancreatic tissue (Fig. 3B). No necrotic tumor tissue was observed in these sections.

Somatostatin Receptor-Binding Studies

Biochemical analysis to determine the presence of high-affinity binding sites for [Tyr^{3}]-octreotide was performed in the primary tumor and in a liver metastasis of Dog 10. There was specific binding of [^{125}I-Tyr^{3}]-octreotide to membranes isolated from both specimens, which could be displaced in a dose-dependent manner with unlabeled [Tyr^{3}]-octreotide (Fig. 4). Scatchard analysis (Fig. 4, inset) of the data revealed a single class of high-affinity binding sites with apparent dissociation constants (Kd) of 1.7 n*M* (primary tumor) and 1.4 n*M* (liver metastasis). The maximum binding capacity (Bmax) was 499 fmol/mg membrane protein (primary tumor) and 537 fmol/mg membrane protein (liver metastasis).

In Vivo Somatostatin Receptor Imaging

In Dogs 5–10 (Table 3) the procedure was performed without problems and [^{111}In-DTPA-d-Phe^{1}]-octreotide caused no side-effects. Nonspecific accumulation of radioactivity was seen in the kidneys of all and in the spleen of one dog (Dog 5) (Fig. 5).

In Dogs 5 and 6 solitary tumors were found in the region of the pancreas without evidence of metastases (Fig. 5). In Dogs 7 and 8 areas of increased uptake were found cranioventral to the left kidney in the region of the pole of the left pancreatic lobe, making localization of the primary tumors in this lobe likely. The presence of several areas of increased uptake suggested metastases in the regional lymph nodes (Fig. 6). Small metas-

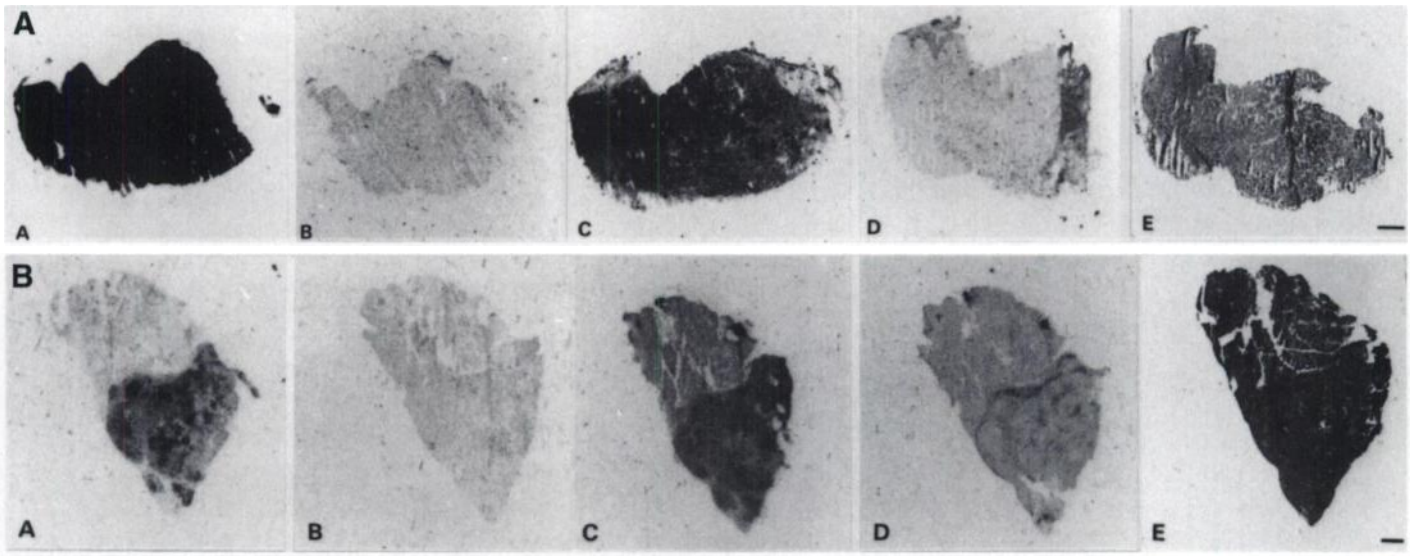

FIGURE 3. (A) Somatostatin receptors in liver metastasis of Dog 10 labeled with either (a) [^{125}I-Tyr^{3}]-octreotide (c) or [^{125}I-Tyr^{11}]-SRIF-14. (a) Autoradiogram on Hyperfilm™-^{3} H showing total binding of [^{125}I-Tyr^{3}]-octreotide. (b) Nonspecific binding in the presence of 1 μM [Tyr^{3}]-octreotide. (c) Autoradiogram on Hyperfilm™-^{3} H showing total binding of [^{125}I-Tyr^{11}]-SRIF-14. (d) Nonspecific binding in the presence of 1 μM [Tyr^{11}]-SRIF-14. (e) Adjacent section stained with hematoxylin and azophloxine. Note the labeling of the insulinomas with both radioligands as well as the displacement with unlabeled peptides. Film exposure time: 4 days; reference bar: 1 mm. (B) Somatostatin receptors in primary tumor of Dog 4. The upper part of each specimen contains normal pancreatic tissue; the lower part contains tumor tissue. Note the absence of SSTRs in the normal pancreatic tissue.

TABLE 3
Test Results in 10 Dogs with Insulinomas

Dog no.	Basal plasma glucose (mmol/liter)	Basal plasma insulin (pmol/liter)	Octreotide test (% of [basal insulin] at 30 min)	In vitro visualization with [^{125}I-Tyr^{11}]-SRIF-14		In vitro visualization with [^{125}I-Tyr^{3}]-octreotide		In vivo imaging with [^{111}In-DTPA]-octreotide	
				Primary tumor	Metastasis	Primary tumor	Metastasis	Primary tumor	Metastasis
1	2.1	804	ND	pos	NA	pos	NA	ND	ND
2	2.1	969	ND	NA	pos	NA	pos	ND	ND
3	2.0	208	31	pos	pos	pos	pos	ND	ND
4	2.2	108	40	pos	NA	pos	NA	ND	ND
5	3.0	215	37	pos	NA	pos	NA	pos	neg
6	2.7	582	42	pos	NA	pos	NA	pos	neg
7	1.6	524	70	ND	pos	pos	pos	pos	pos
8	2.8	1278	79	pos	pos	pos	pos	pos	pos
9	2.3	165	30	pos	pos	pos	pos	pos*	pos
10	1.7	524	26	pos	pos	pos	pos	pos*	pos

*Location of the primary tumor could not be determined because of multiple metastases in the liver and/or regional lymph nodes.

Basal plasma insulin and glucose concentrations (n = 10) were used for the clinical diagnosis of insulinoma. The response of plasma insulin (n = 8) during the octreotide test is expressed as the plasma insulin level at 30 min as a percentage of the level at 0 min. Results of in vitro (n = 10) and in vivo (n = 6) SSTR imaging are presented at pos (the result of the test confirms the presence of the objective) or neg (the result denies the presence of the objective). ND = not done; NA = no tumor tissue available.

tases (<3 mm) found in the liver at necropsy in Dog 7 were not seen on the scan of this dog. Dogs 9 and 10 had multiple areas of increased uptake in the area of the pancreas and liver, indicating metastatic disease. The multiplicity made it impossible to pinpoint the exact location of the primary tumor. Overall, the results of SPECT agreed with findings at surgery and/or necropsy with the exception of the liver metastases in Dog 7. As indicated above, the primary tumors and their metastases visualized in vivo and subsequently removed by surgery and/or at necropsy possessed SSTRs in vitro (Table 3).

DISCUSSION

The clinical data in this report are in agreement with those in previous reports on canine insulinomas (*19–21,28*). Only two of nine primary insulinomas were detected by ultrasonography, and large solitary metastases in regional lymph nodes present in five dogs were not detected. Ultrasonography also has not been very successful in detecting pancreatic tumors in humans, especially when image quality is degraded by intra-abdominal fat or gastrointestinal gas (*29*). Ultrasonography revealed liver metastases in four of the five dogs in which they were present. However, it also revealed other lesions that could be misinterpreted as metastases of insulinoma. In addition, ultrasonography did not detect metastases <3 mm and underestimated the extent of liver metastases. Ultrasonography is, however, readily available and the least expensive of the imaging methods and has additional value in the differential diagnosis of hypoglycemia because it easily reveals large primary liver tumors causing hypoglycemia (*27*). Furthermore, ultrasonography is the technique of choice for the guidance of percutaneous fine-needle aspiration biopsies of visualized masses (*30*).

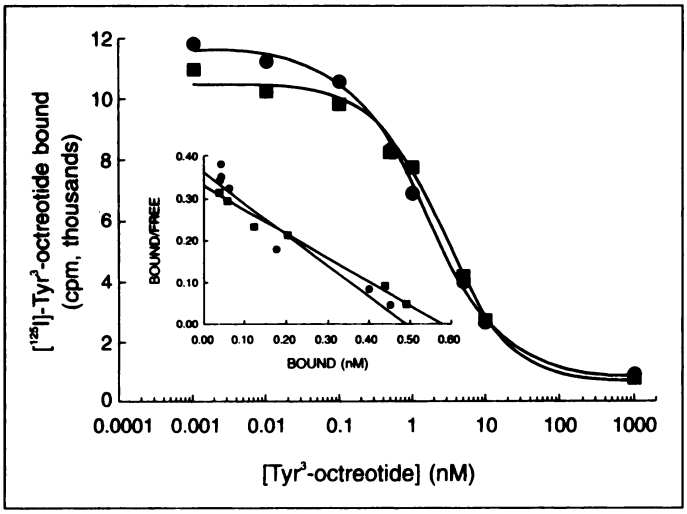

FIGURE 4. Dose-dependent displacement by unlabeled [Tyr^3]-octreotide of [^{125}I-Tyr^3]-octreotide binding in membrane preparations from the primary tumor in Dog 10 (■) and from a metastasis in Dog 10 (●). The incubation time was 60 min. Inset: Scatchard plots of the data.

In dogs with insulinomas, octreotide caused an increase in plasma glucose concentration but usually not to the reference range. Hence the effect of octreotide on glucose concentration was not a dependable indicator of the presence of SSTRs in these insulinomas. The explanation for this lack of a consistent response is unclear, but the co-inhibitory effect of SRIF on the delivery of counterregulatory hormones such as glucagon may play a role (*31*). In patients in which the [^{123}I-Tyr^3]-octreotide scan is negative, there is no rise in plasma glucose concentration after the injection of a single subcutaneous dose of 100 μg octreotide (*32*). The use of octreotide in human subjects having insulinomas with a low affinity for octreotide could even be hazardous, for it could worsen the hypoglycemia as a result of inhibition of the delivery of counterregulatory hormones (*12*). Because plasma glucose levels did not decline during the test and all tumor tissues had SSTRs with high affinity for octreotide, the administration of octreotide appears to be a safe procedure in dogs with insulinomas.

Five subtypes of SSTRs have been distinguished by molecular cloning (*33*). These subtypes show a tissue-specific distribution, differences in the affinity for SRIF and its analogs and a distinct coupling to intracellular effector systems (*34*). In human endocrine pancreatic tumors the in vivo and in vitro effects of octreotide on hormonal release are closely correlated with the presence of SSTRs (*12,13*). The transient suppression of insulin release in the dogs in our study during the octreotide test resembled that in humans with insulinomas (*35*). Basal plasma insulin levels, although varying widely, declined signif-

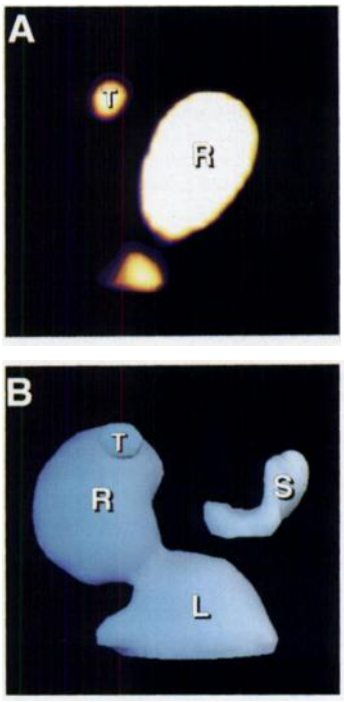

FIGURE 5. SPECT of the upper abdomen of Dog 5 at 6 hr after injection of [^{111}In-DTPA-d-Phe^1]-octreotide. (A) Sagittal image with pathological uptake in a focus (T) ventral to the cranial pole of the right kidney (R). (B) Ventral image of a three-dimensional reconstruction. Note the visualization of the kidneys (L, R) and the spleen (S). In agreement with normal canine anatomy the right kidney (R) is slightly cranial to the left (L). The insulinoma (T) is at the top of the cranial pole of the right kidney. At surgery a pancreatic tumor was found in the right pancreatic lobe at the level of the excretory ducts.

icantly in all dogs after octreotide administration. This suggested that functional SSTRs with high affinity for octreotide were present in all canine insulinomas.

In a subgroup of insulinomas in humans there are receptors with a high affinity for SRIF-14 and SRIF-28 but not for octreotide (*7*). In contrast, autoradiography revealed that all of the canine insulinomas and their metastases bound both [Tyr^3]-octreotide and [Tyr^{11}]-SRIF-14, suggesting the presence of one type of receptor. Biochemical analysis of SSTRs in an insulinoma of one of the dogs showed the presence of high-affinity binding sites for [^{125}I-Tyr^3]-octreotide.

In man, physiological organ accumulation of [^{111}In-DTPA-d-Phe^1]-octreotide is seen in the kidneys, spleen, liver, bladder, thyroid and pituitary (*7*). Radioactivity accumulated in the kidneys and bladders of all dogs and in the spleen of only one dog.

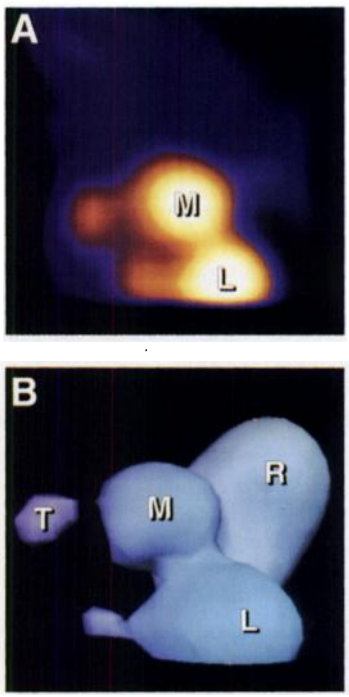

FIGURE 6. - SPECT of the upper abdomen of Dog 7 at 6 hr after injection of [^{111}In-DTPA-d-Phe^1]-octreotide. (A) Sagittal image with pathological uptake in a focus (M) cranial to the left kidney (L). (B) Left lateral image of a three-dimensional reconstruction. There is metastatic tumor in a lymph node (M) between the left (L) and right (R) kidneys. The primary tumor (T) is ventral to this metastasis. At surgery a small (6-mm) primary tumor was found in the left pancreatic lobe, in close proximity to a large metastasis in a splenic lymph node.

The occurrence in humans of a SSTR subtype with a low affinity for octreotide results in the detection of only 63% of the insulinomas by SPECT with [^{123}Tyr^3]-octreotide and [^{111}In-DTPA-d-Phe^1]-octreotide (*7*). In the six dogs with insulinomas in which SPECT was performed with the latter radiopharmaceutical, it detected four of six primary tumors and larger metastases. The location of the other two primary tumors could not be determined because of multiple metastases in the liver and/or regional lymph nodes.

SPECT, as used in this study, detects smaller tumors than do planar images (*11*), but small metastases in the liver could still not be detected. This could be due to attenuation and/or low uptake values. In humans it is customary to perform SPECT 24 hr after the administration of the radiopharmaceutical and again at 48 hr to differentiate between tumor tissue and radioactivity in the bowel contents (*11*). In these dogs SPECT was performed 6 hr after administration of the radiopharmaceutical, before possible interference by radioactivity in the bowel. This had the advantage of avoiding repetition of the anesthesia, but the relatively high background activity may have obscured small lesions.

CONCLUSION

This study suggests that insulinomas and their metastases in dogs express one type of SSTR with a high frequency. This, in combination with the high incidence of metastatic disease, makes canine insulinomas very suitable for the study of the value of SRIF and its analogs in diagnosis and treatment of endocrine pancreatic tumors and their metastases.

ACKNOWLEDGMENTS

We thank Mallinckrodt Medical, Petten, The Netherlands, for their generous gift of [^{111}In-DTPA-d-Phe^1]-octreotide. We thank B.E. Belshaw for critical reading of the manuscript. We acknowledge the technical assistance of Mrs. C.J.C. van Uffelen, Mrs. Y.W.E.A. Pollak and the staff of the Anaesthesiology Division of the Faculty of Veterinary Medicine, Utrecht University, Utrecht, The Netherlands. J.H. Robben received the 'Doko' Scholarship 1992, granted by Spillers Foods B.V., Bunnik, The Netherlands, and H.A. Visser-Wisselaar is supported by grant EUR 94–807 from the Dutch Cancer Society.

REFERENCES

1. Service AJ, McMahon MM, O'Brien PC, Ballard DJ. Functioning insulinoma-incidence, recurrence and long-term survival of patients: a 60-year study. *Mayo Clin Proc* 1991;66:711–719.
2. Pedrazolli S, Pasquali C, Alfano d'Andrea A. Surgical treatment of insulinoma. *Bri J Surg* 1994;81:672–676.
3. Kurosaki Y, Kuramoto K, Murata S, Itai Y. Improved detection of small insulinomas with intravenous dynamic CT. *J Comput Assist Tomogr* 1994;14:588–589.
4. Reubi J-C, Maurer R, von Werder K, Torhorst J, Klijn JGM, Lamberts SWJ. Somatostatin receptors in human endocrine tumors. *Cancer Res* 1987;47:551–558.
5. Reubi J-C, Häcki WH, Lamberts SWJ. Hormone-producing gastrointestinal tumors contain high density of somatostatin receptors. *J Clin Endocrinol Metab* 1987;65: 1127–1134.
6. Reubi J-C, Krenning E, Lamberts SWJ, Kvols L. Somatostatin receptors in malignant tissues. *J Steroid Biochem Molec Bio* 1990;37:1073–1077.
7. Lamberts SWJ, Krenning EP, Reubi J-C. The role of somatostatin and its analogs in the diagnosis and treatment of tumors. *Endocrinol Rev* 1991;12:450–482.
8. Krenning EP, Breeman WAP, Kooij PPM, et al. Localization of endocrine-related tumors with radioiodinated analog of somatostatin. *Lancet* 1989;1:242–244.
9. Bakker WH, Alberts R, Bruns C, et al. [^{111}In-DTPA-d-Phe^1]-octreotide, a potential radiopharmaceutical for imaging of somatostatin receptor-positive tumors: synthesis, radiolabeling and in vitro validation. *Life Sci* 1991;49:1583–1591.
10. Bakker WH, Krenning EP, Reubi J-C, et al. In vivo application of [^{111}In-DTPA-d-Phe^1]-octreotide for detection of somatostatin receptor-positive tumors in rats. *Life Sci* 1991;49:1593–1601.
11. Krenning EP, Kwekkeboom DJ, Bakker WH, et al. Somatostatin receptor scintigraphy with [^{111}In-DTPA-d-Phe^1]- and [^{123}I-Tyr^3]-octreotide: the Rotterdam experience with more than 1000 patients. *Nuklearmedizin* 1993;20:716–731.
12. Lamberts SWJ, Hofland, LJ, van Koetsveld PM, et al. Parallel in vivo and in vitro detection of functional somatostatin receptors in human endocrine pancreatic tumors: consequences with regard to diagnosis, localization and therapy. *J Clin Endocrinol Metab* 1990;71:566–574.

13. Lamberts SWJ, Bakker WH, Reubi J-C, Krenning EP. Somatostatin-receptor imaging in the localization of endocrine tumors. *N Engl J Med* 1990;323:1246–1249.
14. Redding TW, Schally AV. Inhibition of growth of pancreatic carcinomas in animal models by analogs of hypothalamic hormones. *Proc Natl Acad Sci* 1984;81:248–252.
15. Reubi J-C. A somatostatin analog inhibits chondrosarcoma and insulinoma tumor growth. *Acta Endocrinol* 1985;109:108–114.
16. Liebow C, Reilly C, Serrano M, Schally V. Somatostatin analogs inhibit growth of pancreatic cancer by stimulating tyrosin phosphatase. *Proc Natl Acad Sci* 1989;86: 2003–2007.
17. Krenning EP, Kooij PPM, Bakker WH, et al. Radiotherapy with a radiolabeled somatostatin analog, [^{111}In-DTPA-d-Phe^1]-octreotide. *Ann NY Acad Sci* 1994;733: 496–506.
18. Priester WA. Pancreatic islet cell tumors in domestic animals. Data from 11 colleges of veterinary medicine in the United States and Canada. *J Nat Cancer Inst* 1974;53: 227–229.
19. Caywood DD, Klausner JS, O'Leary TP, et al. Pancreatic insulin-secreting neoplasms: clinical, diagnostic and prognostic features. *J Am Anim Hosp Assoc* 1988;24:577–584.
20. Leifer CE, Peterson ME, Matus RE. Insulin-secreting tumor: diagnosis and medical and surgical management in 55 dogs. *J Am Vet Med Assoc* 1986;188:60–64.
21. Dunn JK, Heath MF, Herrtage ME, Jackson KF, Walker, MJ. Diagnosis of insulinomas in the dog: a study of 11 cases. *J Small Animal Pract* 1992;33:514–520.
22. Trinder P. Determination of glucose in blood using glucose oxidase with an alternative oxygen acceptor. *Ann Clin Biochem* 1969;6:24–27.
23. Reubi J-C. New specific radioligand for one subpopulation of brain somatostatin receptors. *Life Sci* 1985;36:1829–1836.
24. Hofland LJ, van Koetsveld PM, Wouters N, Waaijers M, Reubi J-C, Lamberts SWJ. Dissociation of antiproliferative and antihormonal effects of the somatostatin analog octreotide on 7315b pituitary tumor cells. *Endocrinology* 1992;131:571–577.
25. Scatchard G. The attractions of proteins for small molecules and ions. *Ann NY Acad Sci* 1949;51:660–672.
26. Evans HE. The digestive apparatus and abdomen: the pancreas. In: Evans HE, ed. *Miller's anatomy of the dog*, 3rd ed. Philadelphia: W.B. Saunders Co.; 1993:458–460.
27. Leifer CE, Peterson ME, Matus RE, Patnaik AK. Hypoglycemia associated with nonislet cell tumor in 13 dogs. *J Am Vet Med Assoc* 1985;186:53–55.
28. Dunn JK, Bostock DE, Herrtage ME, Jackson KF, Walker HJ. Insulin-secreting tumors of the canine pancreas: clinical and pathological features of 11 cases. *J Small Animal Pract* 1992;34:325–331.
29. Campbell JP, Wilson SR. Pancreatic neoplasms: how useful is evaluation with US. *Radiology* 1988;167:341–344.
30. Hall-Craggs MA, Lees WR. Fine-needle aspiration biopsy: pancreatic and biliary tumors. *Am J Roentgenol* 1986;147:399–403.
31. Reichlin S, Somatostatin (second of two parts). *N Engl J Med* 1983;309:1556–1563.
32. Ur E, Bomanji J, Mather SJ, Britton KE, Wass JAH, Grossman AB, Besser GM. Localization of neuroendocrine tumors and insulinomas using radiolabeled somatostatin analogs, ^{123}I-Tyr^3-octreotide and ^{111}In-pentatreotide. *Clin Endocrinol* 1993;38: 501–506.
33. Kubota A, Yamada Y, Kagimoto S, et al. Identification of somatostatin receptor subtypes and an implication for the efficacy of somatostatin analog SMS 201–995 in treatment of human endocrine tumors. *J Clin Invest* 1994;93:1321–1325.
34. Bruns C, Weckbecker G, Raulf F, et al. Molecular pharmacology of somatostatin-receptor subtypes. *Ann NY Acad Sci* 1994;733:138–146.
35. Lamberts SWJ. Nonpituitary actions of somatostatin. A review on the therapeutic role of SMS 201–995 (sandostatin). *Acta Endocrinol* 1986;276 (suppl):41–55.

Synthesis, Biodistribution and Imaging Properties of Indium-111-DTPA-Paclitaxel in Mice Bearing Mammary Tumors

Chun Li, Dong-Fang Yu, Tomio Inoue, David J. Yang, Wayne Tansey, Chun-Wei Liu, Luka Milas, Nancy R. Hunter, E. Edmund Kim and Sidney Wallace

Division of Diagnostic Imaging and Department of Experimental Radiotherapy, The University of Texas M.D. Anderson Cancer Center, Houston, Texas

Paclitaxel, an antineoplastic agent that stabilizes microtubules and arrests cells in the G2/M cell cycle phase, has shown activity against many common cancers, including ovarian and breast tumors. In order to evaluate the potential value of radiolabeled paclitaxel as an imaging tool in tumors, we synthesized ^{111}In-DTPA-paclitaxel and investigated its biodistribution and gamma scintigraphic imaging properties. **Methods:** Mice bearing a paclitaxel-responsive mammary tumor (MCA-4) were used. DTPA-paclitaxel was labeled with ^{111}In with a radiochemical yield of 84% and radiochemical purity of 90%. Each mouse received 5 μCi of radiotracers intravenously for biodistribution studies and 100 μCi for gamma scintigraphic studies. Indium-111-DTPA was used as a control. **Results:** In tumor-bearing mice, ^{111}In-DTPA was characterized by rapid clearance from the plasma with negligible retention in the tumor, the liver and other body parts. In contrast, ^{111}In-DTPA-paclitaxel exhibited a pharmacological profile resembling that of paclitaxel. Furthermore, a significant uptake of ^{111}In-DTPA-paclitaxel was observed in the tumor. The tumor-to-muscle ratios were 2.64, 3.16 and 6.94 at 30 min, 2 hr and 24 hr, respectively, although absolute uptake in the tumor decreased from 1.95% (injected dose/g) at 30 min to 0.21% at 24 hr after injection. The tumor-to-blood ratio reached 50 at 24 hr after injection. Gamma scintigraphy and autoradiographic studies clearly showed the retention of radiolabeled paclitaxel in the tumor 24 hr after injection. **Conclusion:** These studies suggest that ^{111}In-DTPA-paclitaxel may be clinically useful in studying the uptake of paclitaxel in solid tumors.

Key Words: paclitaxel; biodistribution; gamma scintigraphy; indium-111; DTPA

J Nucl Med 1997; 38:1042–1047

Paclitaxel (Taxol) has shown a remarkable antineoplastic effect in human cancer in Phase I studies and early Phase II and III trials (*1,2*). In advanced ovarian and breast cancer patients who had received multiple prior treatment regimens, response rates of 20%–37% were observed (*2*). Significant activity also has been documented in small-cell and nonsmall-cell lung cancer, head and neck cancers and metastatic melanoma. The antitumor action of paclitaxel is due principally to inhibition of the disassembly of microtubules into tubulin (*1*). Recently, paclitaxel also was shown to be a potent antiangiogenic agent in both normal and tumor-induced angiogenesis (*3*).

The rationale for synthesizing and evaluating indium-labeled paclitaxel is as follows. First, paclitaxel is unique in its mechanism of action as an antimitotic agent and antiangiogenic agent. Given the efficacy of paclitaxel in the treatment of human cancer, the unique binding site for paclitaxel or paclitaxel analogs on the microtubules of the proliferating cells may be an attractive target for selective tumor imaging. As an antiangiogenic agent, radiolabeled paclitaxel may also be used as a tool to image tumor-induced angiogenesis. Second, the

Received Mar. 27, 1996; revision accepted Oct. 2, 1996.

For correspondence or reprints contact: Chun Li, PhD, M.D. Anderson Cancer Center, Department of Diagnostic Radiology, Box 59, 1515 Holcombe Blvd., Houston, TX 77030.